Journal of Molecular Modeling (2020) 26: 278
https://doi.org/10.1007/s00894-020-04523-0

ORIGINAL PAPER

Rotational spectrum simulations of asymmetric tops in an astrochemical context

Julia C. Santos[1] · Alexandre B. Rocha[1] · Ricardo R. Oliveira[1]

Received: 5 June 2020 / Accepted: 26 August 2020 / Published online: 22 September 2020

Abstract

Rotational spectroscopy plays a major role in the field of observational astrochemistry, enabling the detection of more than 200 species including a plethora of complex organic molecules in different space environments. Those line detections allow correctly determining the sources and physical properties, as well as exploring their morphology, evolutionary stage, and chemical evolution pathways. In this context, quantum chemistry is a powerful tool to the investigation of the molecular inventory of astrophysical environments, guiding laboratory experiments and assisting in both line assignments and extrapolation of the experimental data to unexplored frequency ranges. In the present work, we start by briefly reviewing the rotational model Hamiltonian for asymmetric tops beyond the rigid-rotor approximation, including rotational-vibrational, centrifugal, and anharmonic effects. Then, aiming at further contributing to the recording and analysis of laboratory microwave spectroscopy by means of accessible, less demanding quantum chemical methods, we performed density functional theory (DFT) calculations of the spectroscopic parameters of astrochemically relevant species, followed by their rotational spectrum simulations. Furthermore, dispersion-correction effects combined with different functionals were also investigated. Case studies are the asymmetric tops H_2CO, H_2CS, c-HCOOH, t-HCOOH, and HNCO. Spectroscopic parameter predictions were overall very close to experiment, with mean percentage errors smaller than 1% for zeroth order and $\sim$ 5% for first-order constants. We discuss the implications and impacts of those constants on spectrum simulations, and compare line-frequency predictions at millimeter wavelengths. Moreover, theoretical spectroscopic parameters of c-HCOOH and HNCO are introduced for the first time in this work.

Keywords Microwave spectroscopy · Astrochemistry · Asymmetric tops · Rotational spectroscopy

Introduction

A conspicuous attribute of rotational spectroscopy consists in its capability to provide a myriad of information on the molecular species and its environment. Accurate gas-phase structure determinations can be obtained through the analysis of rotationally resolved molecular spectra [1], which provide insight on the species' fine and hyperfine structures by the means of high-resolution techniques such as chirped-pulse [2] and Lamb-dip spectroscopy [3, 4]. Moreover, pioneer laboratory detections of small molecules have been consistently achieved through rotational spectroscopy in the ranges of millimeter and sub-millimeter wavelengths [5–9].

In the field of observational astrochemistry, rotational spectroscopy is majorly employed to unveil the chemical composition and evolution of astrophysical environments. Specially, the interstellar medium (ISM) is known for its chemical lavishness, with radiofrequency line detections of more than 200 species including small hydrocarbons, molecular radicals, and a plethora of complex organic molecules (COMs) to date [10–17]. The analysis of rotational spectra also allows the investigation of the

Electronic supplementary material The online version of this article (https://doi.org/10.1007/s00894-020-04523-0) contains supplementary material, which is available to authorized users.

This paper belongs to Topical Collection *XX-Brazilian Symposium of Theoretical Chemistry (SBQT2019)*

✉ Alexandre B. Rocha
rocha@iq.ufrj.br

Ricardo R. Oliveira
rrodrigues.iq@gmail.com

[1] Instituto de Química, Universidade Federal do Rio de Janeiro, UFRJ, Av. Athos da Silveira Ramos, 149, Rio de Janeiro, RJ 21941-909, Brazil

morphology and evolutionary stage of a particular environment or body [18–20], as well as the determination of its physical properties [21, 22]. Recent technological advances on single dish and interferometry radio antennas have resulted in facilities with remarkable sensitivity and resolution (e.g., the Atacama Large Millimeter Array), consequently increasing the demand for more precise rotational spectroscopic data.

In this context, quantum chemistry is a powerful tool for the investigation of molecular inventory in astrophysical environments. Theoretical predictions of spectroscopic parameters can guide laboratory experiments, assisting in both line assignments and extrapolation of the experimental data to unexplored frequency ranges [5, 9, 11, 23–34]. Moreover, the correct determination of molecular properties such as equilibrium structures from rotational spectra relies greatly on anharmonic vibrational corrections and vibrational-rotational coupling [35]. Quantum-chemical calculations at different levels of theory are therefore of great relevance to contemporary rotational spectroscopy, resulting in a notable increase in published works on the matter vis-à-vis the last century [24, 27, 31, 32, 36–39].

In this work, we focus on a theoretical approach to simulate rotational spectra of asymmetric tops (i.e., rotational constants A ≠ B ≠ C) that correspond to the vast majority of molecules. The reader is referred to specialized literature on other types of rotors (e.g., [40–42] and references therein), which present much simpler energy level structures and consequently much less costly simulations. Although state-of-the-art methods which include complete basis set extrapolations and perturbative quadruple excitation in the coupled-cluster expansion (see Puzzarini et al. [43] and references therein) typically result in very accurate parameters, they are also substantially time-consuming. Consequently, more accessible approaches are beneficial in many different scenarios, Density Functional Theory (DFT) calculations of spectroscopic parameters for four different systems followed by rotational spectrum simulations were performed, aiming at further contributing to accurate and effectively guiding laboratory experiments and, consequently, facilitating the assignment and interpretation of radio spectra from the ISM. For the case studies, the astrochemically relevant species H_2CO, H_2CS, c-HCOOH, t-HCOOH, and HNCO were chosen, most of which are well characterized experimentally. Furthermore, as far as we are concerned, some of the theoretical parameters of c-HCOOH and HNCO are being reported for the first time in this work.

In order to simulate rotational spectra, it is necessary at first to determine the spectroscopic parameters, which are subsequently employed in a simulation of rotational transitions by means of a model Hamiltonian matrix diagonalization. In the section "Theoretical background," some of the theoretical background are discussed with a particular emphasis on the spectroscopic parameters and the necessary approximations to the complete Hamiltonian which are required to simulate the rotational spectra. In the section "Computational details," the computational details are presented. In the section "Results and discussion," results are reported and discussed in detail. Finally, an overview and conclusions are presented in the section "Conclusions."

Theoretical background

The asymmetric rigid rotor

The rotational energy of a rigid rotor is classically expressed as:

$$T_{rot} = \frac{1}{2}(I_a\omega_a^2 + I_b\omega_b^2 + I_c\omega_c^2), \tag{1}$$

where ω_a, ω_b, and ω_c are the angular velocities of the system with respect to the main molecule-fixed axes a, b, and c. The rigid rotor Hamiltonian can therefore be described as a kinetic energy operator expressed in terms of the components of the angular momentum $\hat{\mathbf{J}}$ with relation to the main axes [42]:

$$\hat{H}_{rot} = \frac{1}{2}\frac{\hat{J}_a^2}{I_a} + \frac{1}{2}\frac{\hat{J}_b^2}{I_b} + \frac{1}{2}\frac{\hat{J}_c^2}{I_c} \tag{2}$$

The energies of the rotational levels are the eigenvalues of the Hamiltonian in expression Eq. 2. The unknown asymmetric top eigenfunctions $|\psi_i\rangle$ can be expressed as a linear expansion in terms of a known complete orthonormal set $\{\varphi_i\}$ ($\varphi_i \equiv |J', M', K'\rangle$), which is conveniently chosen as the symmetric top eigenfunctions:

$$|\psi_i\rangle = \sum_{J'}\sum_{M'}\sum_{K'} c^{(i)}_{J',M',K'}|J', M', K'\rangle \tag{3}$$

The sum can be simplified by considering only terms in which the symmetric top quantum numbers J' and M' have the same values of the asymmetric top eigenfunctions ($|\psi_i\rangle$), namely J and M [41]:

$$|\psi_i\rangle = \sum_{K'=-J}^{J} c^{(i)}_{J,M,K'}|J, M, K'\rangle \tag{4}$$

The eigenvalues of $\hat{H}_{rot}$ (Eq. 2) are thus obtained by solving the resulting secular equation, where the symmetric top eigenfunctions φ_i were applied:

$$det[\langle\varphi_m|\hat{H}_{rot}|\varphi_n\rangle - E_i\delta_{mn}] = 0 \tag{5}$$

The quantum number K' gives the angular momentum component along the molecule-fixed axis c for the symmetric top:

$$\hat{J}_c|J, M, K'\rangle = \pm K'|J, M, K'\rangle \quad (6)$$

For asymmetric tops, the double degeneracy of the $\pm K'$ symmetric top quantum numbers is removed, resulting in a splitting of the rotational energy levels and therefore much more complex rotational spectrum profiles [40].

The rotational Hamiltonian beyond the rigid rotor approximation

For simulation purposes in an astrochemical context, corrections to the rotational Hamiltonian beyond the rigid-rotor and harmonic-oscillator approximations ought to be accounted for. The effective rotational Hamiltonian for a given vibrational state is derived from the perturbative treatment of the complete vibrational-rotational Hamiltonian as described by Watson [44], resulting in a transformed Hamiltonian averaged over all vibrational coordinates [45]. This procedure leads to a separation of the rotational and vibrational motions [46], analogous to the splitting between the electronic and vibrational terms of the energy expression in the Born-Oppenheimer approximation.

Hence, the rotational Hamiltonian becomes a function of only the rotational angular momentum operators and vibrationally dependent rotational constants. This effective Hamiltonian can be expressed as a power law whose coefficients are the rotational and centrifugal distortion constants at a particular vibrational state [47–49]:

$$\frac{\hat{H}_{rot}}{hc} = \sum_{\alpha} B_v^{(\alpha)} J_\alpha^2 + 1/4 \sum_{\alpha,\beta} (\tau'_{\alpha\alpha\beta\beta})_v J_\alpha^2 J_\beta^2 + \sum_{\alpha} \Phi_{\alpha\alpha\alpha} J_\alpha^6 + \sum_{\alpha\neq\beta} \Phi_{\alpha\alpha\beta} (J_\alpha^4 J_\beta^2 + J_\beta^2 J_\alpha^4) + \ldots \quad (7)$$

where α and β denote the three main molecule-fixed axes, namely a, b, and c. Ergo, J_α are the components of the total angular momentum along the three main axes in units of $\hbar$. The operator hat notation is henceforth omitted for the sake of simplicity. $B_v^{(\alpha)}$ corresponds to the effective rotational constants, $(\tau'_{\alpha\alpha\beta\beta})_v$ to the effective quartic centrifugal distortion constants as defined by Kivelson and Wilson [50] and $\Phi_{\alpha,\beta,\gamma}$ to the effective sextic centrifugal distortion constants as defined by Watson [48].

The effective Hamiltonian (Eq. 7) can be further simplified by means of contact transformations, since the eigenvalues of a Hamiltonian are unchanged by those operations [51]. Hence, a reduced Hamiltonian [48, 51–53], containing only the linear combinations of the coefficients in Eq. 7, and indistinguishable from the latter in terms of energy levels, is derived.

The reduced Hamiltonian for asymmetric tops as derived by Watson is [51]:

$$\begin{aligned}\frac{\tilde{H}_{rot}^A}{hc} = {} & \sum_{\alpha} B_v^{(\alpha)} J_\alpha^2 - \Delta_J J^4 - \Delta_{JK} J^2 J_z^2 - \Delta_K J_z^4 - 2\delta_J J^2 (J_x^2 - J_y^2) \\ & - \delta_K [J_z^2 (J_x^2 - J_y^2) + (J_x^2 - J_y^2) J_z^2] + H_J J^6 + H_{JK} J^4 J_z^2 \\ & + H_{KJ} J^2 J_z^4 + H_K J_z^6 + 2h_J J^4 (J_x^2 - J_y^2) + h_{JK} J^2 [J_z^2 (J_x^2 - J_y^2) \\ & + (J_x^2 - J_y^2) J_z^2] + h_K [J_z^4 (J_x^2 - J_y^2) + (J_x^2 - J_y^2) J_z^4] + \ldots \end{aligned} \quad (8)$$

where $B_v^{(a)} \equiv A_v$, $B_v^{(b)} \equiv B_v$, and $B_v^{(c)} \equiv C_v$. This reduced Hamiltonian is commonly addressed as Watson's A-type Hamiltonian. For the special case where the rotational constants are accidentally quasi-degenerate and the system approaches a symmetric top, Watson's A Hamiltonian fails [51]. It is thus necessary to employ a different form of the reduced Hamiltonian, namely Watson's S Hamiltonian [49]:

$$\begin{aligned}\frac{\tilde{H}_{rot}^S}{hc} = {} & \sum_{\alpha} B_v^{(\alpha)} J_\alpha^2 - D_J J^4 - D_{JK} J^2 J_z^2 - D_K J_z^4 + d_1 J^2 (J_+^2 + J_-^2) \\ & + d_2 (J_+^4 + J_-^4) + H_J J^6 + H_{JK} J^4 J_z^2 + H_{KJ} J^2 J_z^4 + H_K J_z^6 \\ & + h_1 J^4 (J_+^2 + J_-^2) + h_2 J^2 (J_+^4 + J_-^4) + h_3 (J_+^6 + J_-^6) + \ldots \end{aligned} \quad (9)$$

Vibration-rotation interaction constants

For simplicity, some equations in this section will be expressed solely for the rotational constant B along the b axis, albeit analogous for the other main axes. The asymmetric top rotational constant B_v corrected for the vibrational-rotational coupling of the molecule is expressed as [45]:

$$B_v = B_e - \sum_r \alpha_r^B \left(v_r + \frac{1}{2}\right) + \ldots \quad (10)$$

where B_e denotes the equilibrium rotational constant along the b axis:

$$B_e = \hbar^2 / 2hcI_b \quad (11)$$

The sum in Eq. 10 includes all vibrational normal modes of the system. The vibrational-rotational coupling constant along the b axis α_r^B is derived as [45]:

$$-\alpha_r^B = \frac{2B_e^2}{\omega_r} \left[\sum_{\xi} \frac{3(a_r^{(b\xi)})^2}{4I_\xi} + \sum_{s\neq r} (\zeta_{r,s}^{(b)})^2 \frac{(3\omega_r^2 + \omega_s^2)}{\omega_r^2 - \omega_s^2} + \pi \left(\frac{c}{h}\right)^{1/2} \sum_s \phi_{rrs} a_s^{(bb)} \left(\frac{\omega_r}{\omega_s^{3/2}}\right) \right] \quad (12)$$

where ω_r is the r^{th} harmonic vibrational frequency, corresponding to the Q_r normal mode. The inertial derivatives $a_r^{(\alpha\beta)}$ are defined as:

$$a_r^{(\alpha\beta)} = (\partial I_{\alpha\beta}/\partial Q_r)_e \tag{13}$$

where $I_{\alpha\beta}$ denotes equilibrium moments and products of inertia [54]. The Coriolis zeta constant $\zeta_{r,s}^{(\alpha)}$ couples the normal modes Q_r and Q_s through rotation about the α axis:

$$\zeta_{r,s}^{(\alpha)} = \sum_i \left(L_{ir}^{(\beta)} L_{is}^{(\gamma)} - L_{ir}^{(\gamma)} L_{is}^{(\beta)} \right) \tag{14}$$

where $\mathbf{L}$ corresponds to a matrix that transforms the normal coordinates to mass-weighted Cartesian coordinates. The ϕ_{rst} constants in the third sum of Eq. 12 denote the cubic anharmonic force constants derived from a Taylor expansion of the vibrational potential in terms of the dimensionless normal coordinates q_r, as described by Nielsen [55–57]:

$$\frac{V}{hc} = \frac{1}{2}\sum_r \omega_r q_r^2 + \frac{1}{6}\sum_{rst} \phi_{rst} q_r q_s q_t + \ldots \tag{15}$$

Thus, the vibrational-rotational coupling can be split between two different contributions, the $a_r^{(\alpha\beta)}$ and $\zeta_{r,s}^{(\alpha)}$ constants, which are combined together in a resulting vibrational-rotational parameter $a_r^{(\alpha)}$ (Eq. 12). For an extensive number of molecules, many of the cubic force constants related to stretching modes have negative values, which dominate the expression of $a_r^{(\alpha)}$ for small systems. For this reason, the left side of Eq. 12 is conveniently defined as negative. We should also note that, when two vibrational states are accidentally quasi-degenerate, the Coriolis term in Eq. 12 breaks down, since its perturbative treatment is no longer valid. This configures a special case known as Coriolis resonance, which can be partially solved by neglecting the first-order terms and instead replacing them by [57–59]:

$$(\zeta_{r,s}^{(b)})^2 \frac{(3\omega_r^2 + \omega_s^2)}{\omega_r^2 - \omega_s^2} \rightarrow -\frac{1}{2}(\zeta_{r,s}^{(b)})^2 \frac{(\omega_r - \omega_s)^2}{\omega_s(\omega_r + \omega_s)} \tag{16}$$

Anharmonic vibration constants

The energy levels of a polyatomic molecule can be empirically described by the sum of a vibrational term independent of the rotational quantum numbers and a rotational term parametrically dependent on the vibrational quantum numbers [45]:

$$T(v, J) = G(v) + F_v(J) \tag{17}$$

Similar to the procedure described in the section "The rotational Hamiltonian beyond the rigid rotor approximation," $G(v)$ can be derived by means of a perturbative treatment of the expanded vibrational potential in Eq. (16):

$$G(v) = \sum_r \omega_r \left(v_r + \frac{1}{2}\right) + \sum_r \sum_{s \le r} \chi_{rs} \left(v_r + \frac{1}{2}\right)\left(v_s + \frac{1}{2}\right) + \ldots \tag{18}$$

where χ_{rs} are the anharmonic vibrational constants derived by Nielsen [57]. Following the notation in [45], the diagonal terms of the χ_{rs} matrix are:

$$\chi_{rr} = \frac{1}{16}\phi_{rrrr} - \frac{1}{16}\sum_s \phi_{rrs}^2 \left[\frac{8\omega_r^2 - 3\omega_s^2}{\omega_s(4\omega_r^2 - \omega_s^2)}\right] \tag{19}$$

And for $r \neq s$:

$$\begin{aligned}\chi_{rs} = {} & \frac{1}{4}\phi_{rrss} - \frac{1}{4}\sum_t \left(\frac{\phi_{rrt}\phi_{tss}}{\omega_t}\right) \\ & - \frac{1}{2}\sum_t \left[\frac{\phi_{rst}^2 \omega_t (\omega_t^2 - \omega_r^2 - \omega_s^2)}{\Delta_{rst}}\right] \\ & + \left[A_e(\zeta_{r,s}^{(a)})^2 + B_e(\zeta_{r,s}^{(b)})^2 + C_e(\zeta_{r,s}^{(c)})^2\right]\left[\frac{\omega_r}{\omega_s} + \frac{\omega_s}{\omega_r}\right]\end{aligned} \tag{20}$$

where:

$$\Delta_{rst} = (\omega_r + \omega_s + \omega_t)(\omega_r - \omega_s - \omega_t)(\omega_r + \omega_s - \omega_t)(\omega_r - \omega_s + \omega_t) \tag{21}$$

Those constants can be employed to derive frequencies with the best correspondence to the experimental values, known as the fundamental frequencies ν_r. For an asymmetric top, ν_r are given by the expression [58]:

$$\nu_r = \omega_r + \Delta_r = \omega_r + 2\chi_{rr} + \frac{1}{2}\sum_{s \neq r} \chi_{rs} + \ldots \tag{22}$$

Centrifugal distortion constants

Wilson and Howard [46] described the centrifugal distortion effects as the following term in the rotational Hamiltonian resulting from the perturbative treatment:

$$\sum_{\alpha\beta\gamma\delta} \frac{1}{4}\tau_{\alpha\beta\gamma\delta} J_\alpha J_\beta J_\gamma J_\delta \tag{23}$$

where $\tau_{\alpha\beta\gamma\delta}$ corresponds to:

$$\tau_{\alpha\beta\gamma\delta} = -\frac{1}{2}\sum_r \left(\frac{a_r^{(\alpha\beta)} a_r^{(\gamma\delta)}}{\lambda_r I_\alpha I_\beta I_\gamma I_\delta}\right) \tag{24}$$

Notably, the centrifugal distortion constants (Eq. 24) are, to a good approximation, only functions of the quadratic vibrational potential [52, 58]. The terms in Eq. 24 that have a first-order contribution to the rotational Hamiltonian can be expressed as the centrifugal distortion constant $\tau'_{\alpha\alpha\beta\beta}$ [51, 60, 61]:

$$\tau'_{\alpha\alpha\beta\beta} = \tau_{\alpha\alpha\beta\beta} + 2\tau_{\alpha\beta\alpha\beta}(1-\delta_{\alpha\beta}) \tag{25}$$

Watson demonstrated that only five linear combinations of the six $\tau_{\alpha\beta\gamma\delta}$ constants are directly measurable from experimental spectrum [51, 61]. Those linear combinations are expressed in Watson's A Hamiltonian (Eq. 8) as the five independent quartic centrifugal distortion constants:

$$\begin{aligned}
\Delta_J &= D_J - 2R_6 \\
\Delta_{JK} &= D_{JK} + 12R_6 \\
\Delta_K &= D_K - 10R_6 \\
\delta_J &= \delta_J \\
\delta_K &= -2R_5 - 4\sigma R_6
\end{aligned} \tag{26}$$

The parameters in Eq. 26 are derived by Kivelson and Wilson [60], and are discussed in more detail in Supplementary Information (SI).

In order to obtain the sextic centrifugal distortion correction, it is necessary to perform a perturbative treatment to the fourth order of the complete vibrational-rotational Hamiltonian [44, 62–65]. The ten resulting centrifugal distortion constants can be then rearranged into seven observable independent linear combinations [48, 52, 66]:

$$H_J = \Phi_{600} + 2\Phi_{204} \tag{27a}$$

$$H_{JK} = \Phi_{420} - 12\Phi_{204} + 2\Phi_{024} + 16\sigma\Phi_{006} - 16(R_5 - 2\sigma R_6)s_{111} + 8(2A'_0 - B'_0 - C'_0)s^2_{111} \tag{27b}$$

$$H_{KJ} = \Phi_{240} + \frac{10}{3}\Phi_{420} - 30\Phi_{204} - \frac{10}{3}H_{JK} \tag{27c}$$

$$H_K = \Phi_{060} - \frac{7}{3}\Phi_{420} + 28\Phi_{204} + \frac{7}{3}H_{JK} \tag{27d}$$

$$h_J = \Phi_{402} + \Phi_{006} \tag{27e}$$

$$h_{JK} = \Phi_{222} - 10\Phi_{006} + 4\sigma\Phi_{204} + 2(D_{JK} - 2\sigma\delta_J - 4R_6)s_{111} - 4(B'_0 - C'_0)s^2_{111} \tag{27f}$$

$$h_K = \Phi_{042} + \frac{4}{3}\sigma\Phi_{024} + \left(9 + \frac{32}{3}\sigma^2\right)\Phi_{006} + 4\left[D_K - \frac{2}{3}\sigma R_5 + 2\left(1 + \frac{8}{3}\sigma^2\right)R_6\right]s_{111} + \left(6 + \frac{10}{3}\sigma^2\right)(B'_0 - C'_0)s^2_{111} \tag{27g}$$

The experimental spectra can be adjusted to a particular reduced Hamiltonian by means of the s_{111} parameter. In Watson's A Hamiltonian, s_{111} corresponds to:

$$s_{111} = -\frac{4R_6}{(B'_0 - C'_0)} \tag{28}$$

A detailed description of the $\Phi_{2l,2m,2n}$ parameters can be found in tables IV and VII of the original work by Aliev and Watson [52]. Unlike for quartic centrifugal distortion constants, the sextic constants indeed depend on the cubic vibrational potential. Moreover, the contribution of centrifugal distortion to the effective rotational constants is briefly discussed in the SI.

Transition intensities

Rotational transitions are induced by the interaction of the species' permanent electric dipole moment with the radiation field. The intensities of those transitions are proportional to the square of the dipole moment matrix [67], precluding the observation of pure rotational lines from molecules with no permanent dipole moment. For asymmetric rotors, the dipole moment can be pointed to any arbitrary direction with relation to the main inertial axes. Consequently, the z components of the dipole moment matrix elements can be described as [40]:

$$\mu_z = \mu_a\langle\psi_i|cos(az)|\psi_j\rangle + \mu_b\langle\psi_i|cos(bz)|\psi_j\rangle + \mu_c\langle\psi_i|cos(cz)|\psi_j\rangle \tag{29}$$

Where μ_a, μ_b, and μ_c are the components of the electric dipole moment along the inertial axes, and $\cos(az)$, $\cos(bz)$, and $\cos(cz)$ correspond to the cosines of the angles between the main inertial axes and the space-fixed z axis. The wave functions for asymmetric rotors are denoted as ψ_i.

Computational details

In order to explore the influence of different functionals on rotational spectral simulations, geometry optimization and spectroscopic parameter calculations were performed with the Generalized Gradient Approximation (GGA) functional B97D [68, 69] and the Double-Hybrids (DH) functionals B2PLYP [70] and mPW2PLYP [71]. Grimme's D2 dispersion correction [69] was included in all functionals, and Dunning's aug-cc-pVTZ augmented basis set [72] was used throughout. Geometry optimizations were carried out with Berny's algorithm [73], with 1.5×10^{-5} Hartree/Bohr and 6.0×10^{-5} Angstrom convergence criteria (Gaussian keyword "Opt=Tight"). For all systems, an ultrafine (99,590) integration grid was used (Gaussian keyword "Int=UltraFine"). All calculations were performed with Gaussian 2009 quantum-chemical package [74] and PGOPHER general purpose software [75] was employed on the rotational spectral simulations. All simulated spectra were obtained by considering rotational-vibrational coupling, at VPT2 level, anharmonic and quartic centrifugal-distortion corrections.

For comparison and validation purposes, experimental spectra of H_2CO, H_2CS, c-HCOOH, t-HCOOH, and HNCO were obtained from NASA's Jet Propulsion Laboratory

Table 1 Calculated and experimental spectral parameters of H_2CO

	B2PLYP cc-pVTZ	B2PLYPD aug-cc-pVTZ	B97D aug-cc-pVTZ	mPW2PLYPD aug-cc-pVTZ	Experimental	Martin and Lee (1993)
A_0 (MHz)	283,736.102	282,432.661	277,275.761	283,300.659	281,970.370[a]	282,633.987
B_0	38,766.147	38,714.414	38,526.953	38,912.345	38,835.426	38,465.171
C_0	33,972.283	33,912.840	33,689.527	34,078.056	34,005.730	33,726.651
μ (D)	2.290	2.406	2.257	2.429	2.330[b]	
Δ_J (MHz)	0.0731	0.0738	0.0746	0.0732	0.0755[a]	0.0727
Δ_{JK}	1.2778	1.2947	1.3257	1.2927	1.2936	1.2652
Δ_K	18.8583	18.6700	19.0349	18.6516	19.9782	18.6093
δ_J	0.0097	0.0098	0.0101	0.0097	0.0104	0.00956
δ_K	0.9090	0.9179	0.9439	0.9162	1.0349	0.8963
$H_K \times 10^{-3}$ (MHz)	3.810	3.828	4.149	3.793		3.789
$H_{KJ} \times 10^{-5}$	1.112	1.440	0.7980	1.489		−5.810
$H_{JK} \times 10^{-5}$	2.554	2.605	2.794	2.588		2.580
$H_J \times 10^{-8}$	8.624	8.592	9.752	8.911		8.994
$h_J \times 10^{-8}$	4.042	4.102	4.460	4.126		2.998
$h_{JK} \times 10^{-5}$	1.368	1.395	1.492	1.388		1.370
$h_K \times 10^{-3}$	1.194	1.208	1.275	1.199		1.156

Theoretical values at CCSD(T) level of theory are taken from Martin and Lee (1993)[81]

[a]Experimental effective rotational constants and quartic centrifugal distortion constants obtained from [82] and values therein

[b]Experimental electric dipole moment from [83]

(JPL) database[1] and the Cologne Database for Molecular Spectroscopy (CDMS)[2].

Results and discussion

H_2CO

Formaldehyde (H_2CO) was one of the first molecules to be detected with radiotelescopes [66], and has since been widely observed toward interstellar and circumstellar environments [76–79]. It is commonly used to study the physical conditions of astrophysical sources, acting as a probe for gas temperature and density [80]. In Table 1, calculated and experimental spectroscopic parameters of H_2CO are presented. Theoretical rotational constants corrected for vibrational-rotational effects (hereafter "effective rotational constants," see Eqs. 10 and 12) show excellent agreement with experimental values, with mean discrepancies of 0.3% for all hybrid functionals and $\sim$ 1% for B97D. Centrifugal corrections to the rotational constants as described in equation S4 result in relative changes up to 0.001% for all case studies, and therefore were neglected in order to allow comparison with other theoretical works where only vibrational-rotational corrections were reported. For the quartic centrifugal distortion constants, mean errors of $\sim$ 4% were achieved. Moreover, both hybrid functionals yielded spectroscopic constants generally closer to experiment than CCSD(T) calculations from ref. [81]. Those results demonstrate that the methods and models used here describe very well the formaldehyde parameters and spectrum, with a slightly better performance of the B2PLYP functional with dispersion corrections. Although an already small mean error of $\sim$ 0.3% is achieved for the effective rotational constants at the B2PLYP/cc-pVTZ level of theory, with the addition of dispersion corrections and diffuse functions, this error is further improved to ∼0.25%. Similarly to B2PLYP, calculations with the mPW2PLYP functional with dispersion corrections yielded errors of $\sim$ 0.29%, evincing the generally good performance of hybrid functionals at spectroscopic parameter determinations. Overall, D2 dispersion corrections and augmented basis sets have shown better accuracy with respect to the measured constants, suggesting that those effects should be included in the theory even for tightly bounded molecules such as H_2CO [58]. Nevertheless, the B97D/aug-cc-pVTZ level yielded the largest errors for the effective rotational constants, and centrifugal distortion constants only slightly better than B2PLYP/cc-pVTZ, despite accounting for dispersion effects.

[1]Available in https://spec.jpl.nasa.gov/ftp/pub/catalog/catdir.html

[2]Available in https://cdms.astro.uni-koeln.de/cdms/portal/

Although all centrifugal distortion constants are generally difficult to derive theoretically, the δ_K constant is specially sensitive to the level of theory [58], leading to systematically larger discrepancies in comparison with the other quartic constants. Moreover, as discussed by Clabo et al. [58], the experimental value for δ_K is not completely consistent with the other measured constants. From the experimental values for Δ_J, Δ_{JK}, Δ_K, and δ_J, and by assuming planarity conditions [84], one can derive the experimental τ constants that, subsequently, yield $\delta_K = 0.9277$ MHz. This value is much closer to the predicted δ_K for all levels of theory, with a mean relative error smaller than 1%. Thus, the current theoretical formulation for the δ_K constant indeed seems not to describe, to a good extent, the phenomenological parameter δ_K obtained from experiments.

In what concerns spectral simulations, even slight differences in accuracy for the effective rotational constants are of great relevance to accurately predict line frequencies, since those constants have a zeroth-order contribution to the rotational energy. The simulated spectrum of formaldehyde at 300K with mPW2PLYPD/aug-cc-pVTZ level of theory is shown in Fig. 1, in comparison with the experimental spectrum from the JPL database. The simulation was truncated at a maximum upper J value of 57, and Watson's A Hamiltonian was employed. Sextic centrifugal distortion constants are difficult to determine both theoretically and experimentally, and thus were not included in the simulations. For transitions with lower J values (< 800 GHz), discrepancies between experimental and theoretical frequencies with mPW2PLYPD functional were around $\sim$ 1.00 GHz ($\sim$ 0.13% in relative terms). It is worth emphasizing that this frequency range corresponds to the relevant region for astronomical radio-observations. Comparatively, B2PLYP/cc-pVTZ (Fig. S1) and B2PLYPD/aug-cc-pVTZ (Fig. S2) yielded errors of $\sim$ 0.53 and $\sim$ 1.3 GHz, respectively. Although the B2PLYP functional predicted the most accurate rotational frequencies for this system, the overall best performing functional for asymmetric tops was mPW2PLYP, as will be discussed in Sections H_2CS, HCOOH, and HNCO. This apparently contradictory result can be understood by analyzing each effective rotational constant separately. For B2PLYPD/aug-cc-pVTZ, the A_0 constant yielded a relative error of $\sim$ 0.16%, which was considerably closer to experiment than for B2PLYP/cc-pVTZ ($\sim$ 0.62%) and mPW2PLYPD/aug-cc-pVTZ ($\sim$ 0.47%). However, the B_0 and C_0 constants predicted by B2PLYP with dispersion corrections were less accurate than both other levels of theory. In fact, the B2PLYP/cc-pVTZ description achieved the most accurate B_0 and C_0 constants, which consequently leads to better frequency predictions. Indeed, for formaldehyde, the A_0 effective rotational constant seems to be the least dominant regarding rotational spectrum simulations. This result demonstrates that one must be attentive of all rotational constants separately when performing spectrum simulations. It should also be noted that both B_0 and C_0 constants obtained from CCSD(T) calculations by ref. [81] were on average $\sim$ 350 MHz further from experiment in comparison with hybrid DFT results.

This outcome is suited to guide laboratory experiments of recording and analyzing microwave spectra which play a key role in the fields of radioastronomy and astrochemistry.

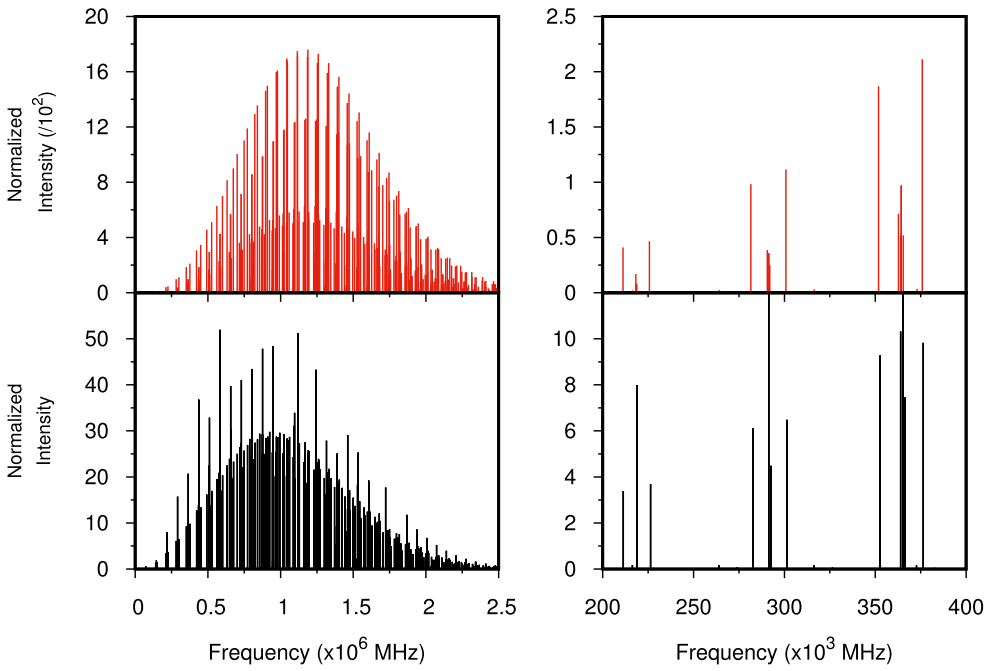

Fig. 1 Rotational spectrum of H_2CO at 300 K simulated with mPW2PLYPD/aug-cc-pVTZ level of theory (black). The experimental spectrum is shown in red. In the right panel, an astronomical relevant region is zoomed in

The simulated spectrum at B97D/aug-cc-pVTZ level of theory is shown in Fig. S3. The vibrational-rotational coupling constants (see Eq. 12) at the mPW2PLYP/aug-cc-pVTZ level of theory for all case studies are also listed in the SI.

H_2CS

Since the 1970s, sulfur-containing molecules have been observed to be depleted in dense regions of the ISM in comparison with cosmic abundances [85–88], while in diffuse and highly ionized regions their abundances are seemingly cosmic [89–93]. Inasmuch as the sulfur chemical sink has yet to be identified, this phenomenon, namely the sulfur depletion problem [94], has been arousing much interest of the astrochemical community toward sulfur-bearing molecules. As a relevant example, thioformaldehyde (H_2CS) is a slightly asymmetric rotor that has been observed toward several interstellar sources [22, 95–99]. However similar in structure to its oxygen analogue H_2CO, thioformaldehyde has much less optically thick lines, therefore being a good alternative to determine the physical properties of a particular source. Two main formation routes have been suggested for this molecule, resulting from either reactions involving atomic sulfur and the methyl radical (CH_3) in hot cores [100], or forming on the surface of grain mantles within dense molecular clouds [88].

Theoretical and experimental spectroscopic parameters of H_2CS are listed in Table 2. While all functionals derived effective rotational constants close to experiment (with relative mean errors less than 1%), B97D yielded slightly less accurate results than the hybrid functionals. However, its predictions of the quartic centrifugal distortion constants were the closest to experiment, again evincing an apparent advantage of the GGA functional in describing the quadratic force field of asymmetric tops. Martin et al. [101] have derived theoretical values for the spectroscopic constants of H_2CS with CCSD(T) calculations, which are listed in Table 2. As for H_2CO, the parameters obtained through DFT calculations were comparable with the predictions of the coupled-cluster approach, but with much less demanding computational effort. The exceptions are the H_{KJ}, h_{JK}, and h_K sextic centrifugal distortion constants, whose DFT predictions deviate more than one order of magnitude from the CCSD(T) calculations, possibly due to the higher difficulty associated with their derivation [102, 103].

From the experimental Δ_J, Δ_{JK}, Δ_K, and δ_J, we derive a new $\delta_K = 0.3326$ MHz. For this new value, the mean

Table 2 Calculated and experimental spectral parameters of H_2CS

	B2PLYP cc-pVTZ	B2PLYPD aug-cc-pVTZ	B97D aug-cc-pVTZ	mPW2PLYPD aug-cc-pVTZ	Experimental	Martin et al. (1994)
A_0 (MHz)	293,888.436	293,079.382	289,947.613	294,311.184	291,613.519[a]	293,547.182
B_0	17,593.668	17,574.772	17,476.466	17,656.413	17,699.7198	17,776.928
C_0	16,563.637	16,544.104	16,446.043	16,620.665	16,651.7382	16,762.086
μ (D)	1.724	1.759	1.733	1.774	1.649[b]	
Δ_J (MHz)	0.01867	0.01879	0.01917	0.01859	0.019358[a]	0.0187
Δ_{JK}	0.51451	0.51821	0.52730	0.51557	0.52095	0.51145
Δ_K	22.37431	22.34474	22.94792	22.30371	23.3260	22.0590
δ_J	0.00110	0.00111	0.00114	0.00110	0.00120457	0.00109
δ_K	0.32309	0.32524	0.33313	0.32427	0.37195	0.31966
$H_K \times 10^{-3}$ (MHz)	5.316	5.369	5.840	5.273	5.483	5.2311299
$H_{KJ} \times 10^{-5}$	−0.2482	−0.1005	−0.2700	−0.09278		−3.900519
$H_{JK} \times 10^{-6}$	3.744	3.783	4.036	3.756		3.56776
$H_J \times 10^{-10}$	11.05	9.543	8.529	15.52		2.5
$h_J \times 10^{-9}$	1.704	1.718	1.800	1.733		1.62
$h_{JK} \times 10^{-6}$	2.114	2.136	2.265	2.119		657.68837
$h_K \times 10^{-4}$	6.742	6.816	7.176	6.754		0.0201943

Theoretical values at CCSD(T) level of theory are taken from Martin et al. [101]

[a]Experimental effective rotational constants and quartic centrifugal distortion constants obtained from [104]

[b]Experimental electric dipole moment from [105]

relative errors of the δ_K constants obtained with all three functionals corrected for dispersion effects ranged from 0.16 to 2.5%. Those discrepancies were systematically lessened by around 10% when compared with the measured constant, once more supporting the hypothesis of a faulty theoretical description of the δ_K constant.

The best performing functional for H_2CS was mPW2PLYP, which yielded mean errors of $\sim$ 0.45% for the effective rotational constants and $\sim$ 6.20% for the quartic centrifugal distortion constants. The simulated spectrum of thioformaldehyde at 300K with this functional is shown in Fig. 2, in comparison with the experimental spectrum from the JPL database. Watson's A Hamiltonian was employed in the simulation, with $J_{max} = 27$. Again, sextic centrifugal distortion constants were neglected. The simulated spectra at B2PLYPD/aug-cc-pVTZ and B97D/aug-cc-pVTZ levels of theory are shown in the SI.

For J values up to 10, simulated transitions at the mPW2PLYPD/aug-cc-pVTZ level of theory yielded errors ranging from $\sim$ 200 to $\sim$ 675 MHz. Comparatively, the mean discrepancies for the same low J interval at B2PLYPD and B97D levels of theory were, respectively, $\sim$ 1500 MHz and $\sim$ 2700 MHz. Notably, accurate predictions of the rotational constants are fundamental to the spectrum simulations. In particular, the B_0 and C_0 constants have repeatedly proven to play a key role on the frequency calculation of the rotational transitions of molecules with C_{2v} symmetry. Moreover, the B_0 and C_0 rotational constants obtained with CCSD(T) calculations were considerably further from experiment than those predicted by the mPW2PLYPD functional.

HCOOH

The first detections of formic acid (HCOOH) in the interstellar medium were reported by Zuckerman et al. (1971) [106] and Winnewisser and Churchwell (1975) [107] toward the Giant Molecular Cloud (GMC) Sgr B2. Thenceforth, both rotational isomers have been detected toward a variety of sources such as high- and low-mass star-forming regions and protoplanetary disks [108–110]. Its structural similarities to more complex, biologically important species such as amino acids give formic acid a distinctive role in the field of astrobiology. Indeed, chemical routes to form glycine from HCOOH have been explored since the 1970s (e.g., [111–113]). In the present work, we have obtained the spectroscopic parameters and simulated rotational spectra for the *cis* and *trans* rotamers of HCOOH. Both isomers have C_s-symmetry, with an energy difference of 16.3 kJ mol^{-1} between them [114]. It should be noted, however, that since both rotamers are in equilibrium at 300K, their rotational spectrum measurements are virtually inseparable. The determination of their respective rotational frequencies and spectroscopic parameters from experiment must then be performed by means of separate fittings of the intensity-weighted lines within the conjoined spectrum. Thus, caution is necessary when comparing experiment and theory for these species.

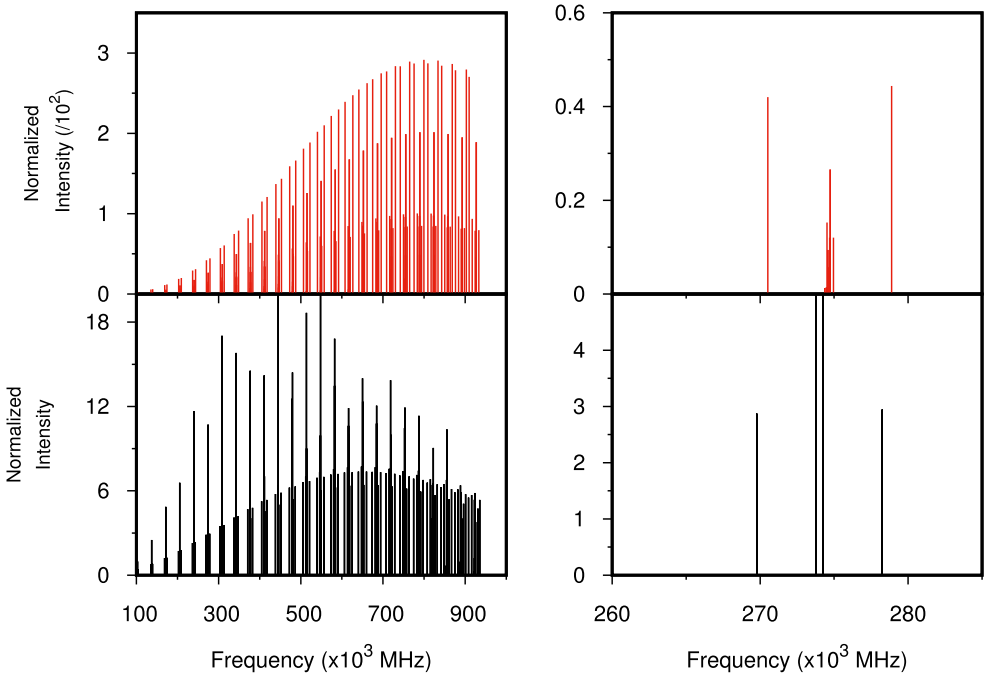

Fig. 2 Rotational spectrum of H_2CS at 300 K simulated with mPW2PLYPD/aug-cc-pVTZ level of theory (black). The experimental spectrum is shown in red. In the right panel, an astronomical relevant region is zoomed in

Table 3 presents the calculated and experimental spectroscopic parameters of c-HCOOH. Considering the main terms of the rotational energy expression, the best performance was achieved by the mP2WPLYPD/aug-cc-pVTZ level of theory, with a relative error of ∼ 0.29% for the effective rotational constants and ∼ 2.9% for the quartic centrifugal distortion constants. Comparatively, the B2PLYP/cc-pVTZ and B2PLYPD/aug-cc-pVTZ levels of theory yielded errors of, respectively, ∼ 0.54% and ∼ 0.60% for the effective rotational constants. While the incorporation of dispersion corrections and diffuse functions to the B2PLYP functional resulted in a difference of ∼ 460 MHz in the rotational constant A_0 toward the experimental value, it also led to B_0 and C_0 values ∼ 10 MHz further from experiment. Conversely, mPW2PLYPD/aug-cc-pVTZ obtained both B_0 and C_0 constants ∼ 45 MHz closer than B2PLYP/cc-pVTZ to the measurements. Moreover, dispersion corrections have considerably improved the quartic centrifugal distortion constants with all functionals, as one would expect. The B97D/aug-cc-pVTZ level of theory yielded quartic centrifugal distortion constants closest to experiment, with a mean error of ∼ 2.4%. However, its larger discrepancies for the effective rotational constants (∼ 1.7%) make this functional the least adequate to perform spectrum simulations. Regardless of the choice of functional, however, the sextic centrifugal distortion constants show great variance on accuracy (with relative errors ranging from ∼ 11 to ∼ 100% depending on the coefficient). Nonetheless, considering the small absolute magnitude of those constants and their high dependency on the theory level against a relatively small contribution to the rotational energy, higher errors are expected and rather tolerated.

Predicted and measured constants for the t-HCOOH are listed in Table 4. In this work, the effective rotational constants of the *trans* rotamer were also best predicted by the mPW2PLYPD/aug-cc-pVTZ level of theory, again with a mean relative error of ∼ 0.29%. Comparatively, the effective rotational constants obtained by Demaison et al. [115] with CCSD(T)/cc-pVTZ calculations yielded relative errors of ∼ 0.7%. As for the *cis* rotamer, B_0 and C_0 rotational constants calculated with mPW2PLYPD were displaced around 40 MHz toward the experimental value in comparison with B2PLYPD. For this configuration, the addition of diffuse functions and dispersion corrections to the B2PLYP functional were much less impactful than for the *cis* rotamer, only improving the A_0 rotational constant in the B2PLYPD/aug-cc-pVTZ level of theory by ∼100 MHz. Nevertheless, distinctions between the behaviors of each isomer could be largely influenced by the difficulty in dissociating their experimental spectra. The GGA functional yielded effective rotational constants with a mean relative error of ∼ 1.8%, the worst performance between all functionals. Regarding centrifugal effects, the

Table 3 Calculated and experimental spectral parameters of c-HCOOH

	B2PLYP cc-pVTZ	B2PLYPD aug-cc-pVTZ	B97D aug-cc-pVTZ	mPW2PLYPD aug-cc-pVTZ	Experimental[a]
A_0 (MHz)	86,703.563	86,242.515	85,059.319	86,768.958	86,461.624
B_0	11,604.990	11,596.418	11,472.794	11,654.416	11,689.185
C_0	10,211.191	10,208.034	10,094.924	10,260.528	10,283.996
μ (D)	3.858	3.908	3.755	3.941	3.790
Δ_J (MHz)	0.00813	0.00824	0.00860	0.00816	0.00836
Δ_{JK}	−0.06967	−0.06979	−0.06742	−0.07026	−0.07144
Δ_K	2.38676	2.38092	2.39963	2.38177	2.36167
δ_J	0.00136	0.00138	0.00143	0.00137	0.00142
δ_K	0.03808	0.03841	0.04021	0.03813	0.04075
$H_K \times 10^{-4}$	1.639	1.644	1.722	1.629	1.851
$H_{KJ} \times 10^{-6}$	−4.348	−4.466	−4.764	−4.338	−9.673
$H_{JK} \times 10^{-7}$	−3.751	−3.891	−4.485	−3.787	−2.974
$H_J \times 10^{-9}$	5.768	5.719	5.377	5.798	10.64
$h_J \times 10^{-9}$	5.071	5.180	5.525	5.129	2.317
$h_{JK} \times 10^{-8}$	5.529	5.331	5.073	5.511	−73.00
$h_K \times 10^{-5}$	1.431	1.440	1.499	1.428	

[a][116]

Table 4 Calculated and experimental spectral parameters of t-HCOOH

	B2PLYP cc-pVTZ	B2PLYPD aug-cc-pVTZ	B97D aug-cc-pVTZ	mPW2PLYPD aug-cc-pVTZ	Experimental [a]	CCSD(T) [b] cc-pVTZ
A_0 (MHz)	77,194.408	77,021.950	76,693.034	77,300.596	77,512.235	77,377.000
B_0	11,978.294	11,953.367	11,775.965	12,023.530	12,055.106	11,934.067
C_0	10,345.289	10,323.635	10,184.043	10,381.245	10,416.115	10,322.786
μ (D)	1.465	1.511	1.506	1.528	1.420	
Δ_J (MHz)	0.00836	0.00834	0.00838	0.00832	0.009996	0.00973
Δ_{JK}	0.15283	0.15321	0.17484	0.15033	−0.086249	-0.08872
Δ_K	1.2160	1.2321	1.3088	1.2212	1.702447	1.69560
δ_J	0.00117	0.00116	0.00110	0.00117	0.001949	0.00189
δ_K	0.09748	0.09723	0.10243	0.09654	0.042732	0.03863
$H_K \times 10^{-5}$	4.589	4.682	5.037	4.626	12.12	11.73
$H_{KJ} \times 10^{-6}$	1.373	1.066	1.686	1.089	−10.57	−9.2
$H_{JK} \times 10^{-6}$	1.212	1.241	1.367	1.217	0.102	0.013
$H_J \times 10^{-9}$	−2.394	−1.975	−2.838	−1.872	13.14	10.3
$h_J \times 10^{-9}$	1.166	1.349	1.247	1.360	5.763	7.3
$h_{JK} \times 10^{-7}$	6.115	6.379	7.162	6.236	0.9750	1.3
$h_K \times 10^{-5}$	2.567	2.575	2.841	2.531	1.482	1.3

[a][116]
[b][115]

B2PYLP/aug-cc-pVTZ level of theory predicted the most accurate quartic centrifugal distortion constants, although for the t-HCOOH rotamer the calculated values were much farther from the experimental data than for c-HCOOH. In particular, the Δ_{JK} and δ_K constants predictions yielded relative errors of more than 100%, whereas for the other quartic constants the relative errors were around 25%. Furthermore, Demaison et al. [115] obtained quartic and sextic centrifugal distortion constants comparatively closer to experiments.

As for H_2CO, the inconsistency of the δ_K constant was investigated. From the planarity conditions and the experimental values for the other quartic centrifugal distortion constants, one can obtain $\delta_K = 0.0378$ MHz for c-HCOOH and $\delta_K = 0.0400$ MHz for t-HCOOH. For the *cis* rotamer, the derived experimental value of δ_K was again generally closer to the theoretical predictions, yielding mean relative errors of $\sim$ 1%. The exception was the B97D/aug-cc-pVTZ level of theory, which predicted a δ_K constant that was closer to measurements. For the *trans* isomer, however, the τ constants (Eq. 24) seem to be less accurately described by the theory, and as a result the discrepancies of the Δ_{JK} and δ_K predictions were unusually large. Thus, the "corrected" value for δ_K is still rather different from the calculations, since the latter are directly affected by the seemingly amiss τ constants.

The simulated spectra of c-HCOOH and t-HCOOH at the mPW2PLYP/aug-cc-pVTZ level of theory are shown in Figs. 3 and 4, while the spectra simulated at the B2PLYPD/aug-cc-pVTZ and B97D/aug-cc-pVTZ levels of theory are presented in the SI. For the c-HCOOH rotamer, experimental transitions were obtained from the CDMS catalog, while for t-HCOOH the experimental spectrum was available at JPL. All simulations were performed with Watson's A-type Hamiltonian, truncating a J maximum of 100 for the *cis* and 20 for the *trans* rotamer.

For c-HCOOH at low J values ($< J = 10$), predicted frequency errors were around 100 MHz for the mPW2PLYP/aug-cc-pVTZ level of theory, ranging from $\sim$13 to $\sim$195 MHz. The mean errors associated with B2PLYP/cc-pVTZ and B2PLYPD/aug-cc-pVTZ were, respectively, $\sim$ 348 and $\sim$ 971 MHz. These results suggest that, similarly to H_2CO and H_2CS, the B_0 and C_0 effective rotational constants are much more relevant to the rotational energy levels of c-HCOOH than the A_0 constant. Although the B97D functional was the best for describing the quartic centrifugal distortion constants, frequency errors for this system even at low J values were approximately 3 GHz, much larger than for all the other levels of theory. Ergo, the larger discrepancies in the effective rotational constants predicted with B97D have much more influence than centrifugal corrections to the energy levels. Again,

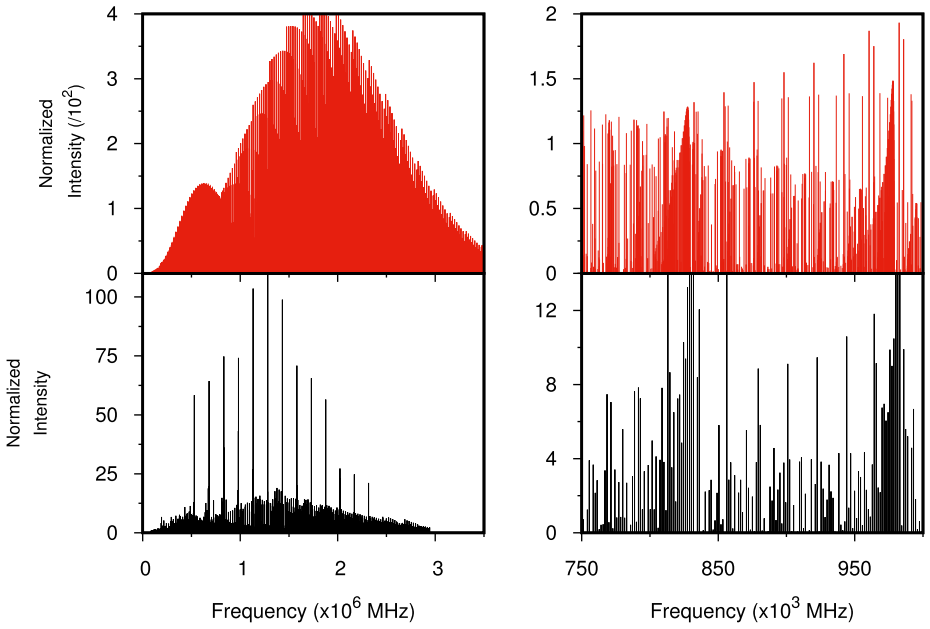

Fig. 3 Rotational spectrum of c-HCOOH at 300 K simulated with mPW2PLYPD/aug-cc-pVTZ level of theory (black). In the right panel, an astronomical relevant region is zoomed in. The experimental spectrum is shown in red

it becomes evident that accurate rotational constants are fundamental to correctly predict rotational frequencies.

For t-HCOOH, the mPW2PLYP/aug-cc-pVTZ level of theory predicted frequencies with a mean error of 614 MHz at low J values, and B2PLYPD/aug-cc-pVTZ yielded errors of $\sim$ 1.47 GHz. Notably, frequency discrepancies for t-HCOOH were significantly higher than for the *cis* rotamer, despite both configurations presenting effective rotational constants similarly well described by theory. Thus, it is likely that the substantial difference between frequency prediction errors for each rotamer is due to the effectiveness of the functionals to describe the system's quadratic force field, and consequently to determine its centrifugal distortion effects. Nevertheless, the mPW2PLYP/aug-cc-pVTZ has consistently achieved the best theoretical frequencies for HCOOH, with sufficiently good predictions to guide microwave spectroscopy measurements.

For both HCOOH isomers, but especially for the *cis* rotamer, transition intensity predictions deviated considerably from the measured spectra. This result is unexpected, since both yielded permanent dipole moments fairly close to experiments with all functionals. Precisely, while the experimental values for the two dipole moment components of c-HCOOH are listed as $\mu_a = 2.65$ D and

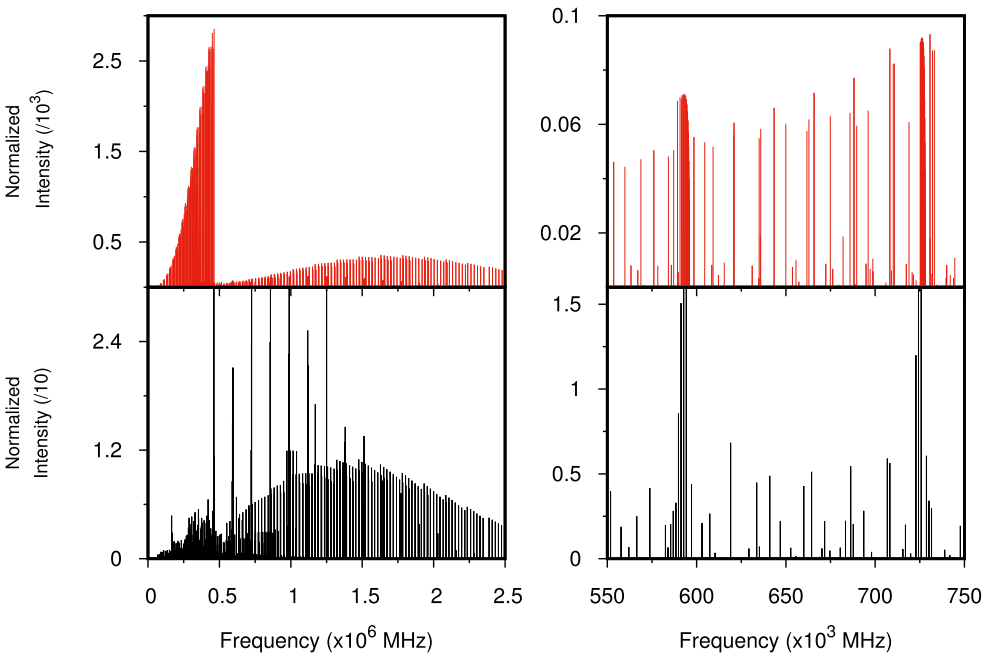

Fig. 4 Rotational spectrum of t-HCOOH at 300 K simulated with mPW2PLYPD/aug-cc-pVTZ level of theory (black). In the right panel, an astronomical relevant region is zoomed in. The experimental spectrum is shown in red

μ_b = 2.71 D [114], the mPW2PLYPD/aug-cc-pVTZ calculations derived μ_a = 2.80 D and μ_b = 2.77 D, the least accurate among all functionals. Indeed, semi-empirical simulations of c-HCOOH rotational spectrum where the experimental dipole moment components were employed also result in the same spectral profile as derived with the theoretical parameters.

HNCO

Isocyanic acid (HNCO), the smallest molecule containing the four biogenic elements, was first detected in the interstellar medium toward the GMC Sgr B2 [117–119]. Since then, it has been detected toward multiple different environments, ranging from high- and low-mass protostars to extragalactic sources [22, 120–124]. The main formation pathway for this molecule in hot cores consists in gas-phase neutral-neutral reactions: complex organic molecules formed from HNCO evaporate from grain mantles to the gas phase, where they suffer dissociation processes leading to the production of HNCO [122, 125]. As a consequence, numerous works have suggested that HNCO could trace large-scale shocks, giving insight on the source's morphology [125–127].

In Table 5, calculated and experimental spectroscopic constants of HNCO are listed. The mean relative errors of the effective rotational constants yielded by the functionals B2PLYPD, B97D and mPW2PLYPD were, respectively, ∼ 4.2%, ∼ 6.1%, and ∼ 3.1%. Those unusually large errors are predominantly associated with the A_0 constant, which was generally poorly predicted in comparison with the other case studies. As for H_2CS and HCOOH, the best predictions were achieved by the mPW2PLYPD/aug-cc-pVTZ level of theory, whereas the effective rotational constants calculated with the GGA functional were the furthest from experiment. Nonetheless, all three functionals yielded better predictions than calculations at the CISD level of theory reported by Ref. [128]. Centrifugal distortion is large for HNCO, and as a consequence its constants were particularly difficult to predict, with discrepancies as big as three orders of magnitude compared with the measurements.

Isocyanic acid constitutes a quasi-symmetric rotor, given that the B_0 and C_0 rotational constants are accidentally quasi-degenerate. Thus, the S-reduction of Watson's Hamiltonian [49] was employed in the simulation. Figure 5 shows the predicted spectrum of HNCO at the mPW2PLYP/aug-cc-pVTZ level of theory and the experimental spectrum from the JPL database. The simulation was performed at T= $300K$, with J_{max} = 47 and sextic centrifugal distortion constants were not included. Intensity units were set to arbitrary due to an overflow of the Boltzmann expression at high J levels, which is a direct consequence of the large

Table 5 Calculated and experimental spectral parameters of HNCO

	B2PLYP cc-pVTZ	B2PLYPD aug-cc-pVTZ	B97D aug-cc-pVTZ	mPW2PLYPD aug-cc-pVTZ	Experimental	CISD
A_0 (MHz)	1,006,272.618	1,022,565.218	1,075,036.194	994,939.517	918,504.400[a]	818,424.000
B_0	11,145.126	11,138.053	11,089.834	11,179.388	11,071.008	10,911.000
C_0	10,861.358	10,851.251	10,785.718	10,904.344	10,910.576	10,768.000
μ (D)	2.109	2.079	2.034	2.090	2.070[b]	
Δ_J (MHz)	0.00260	0.00259	0.00251	0.00265	0.003486[a]	
Δ_{JK}	15.9048	16.4925	18.3726	15.1341	0.931700	
Δ_K	5906.15	6428.21	8876.09	5034.28	6065.60	
δ_J	0.00027	0.00028	0.00034	0.00024	−0.000073	
δ_K	0.00009	−0.00009	−0.00010	−0.00008	−0.000037	
$H_K \times 10^{+2}$ (MHz)	1.243	1.463	2.830	0.8876	2.876	
$H_{KJ} \times 10^{-1}$	4.209	4.718	7.331	3.370	0.3229	
$H_{JK} \times 10^{-4}$	1.647	1.754	2.153	1.500	0.02490	
$H_J \times 10^{-9}$	−4.227	−4.295	−4.270	−4.181		
$h_J \times 10^{-9}$	−2.631	−2.695	−2.857	−2.548		
$h_{JK} \times 10^{-11}$	−2.213	−3.404	−10.68	1.201		
$h_K \times 10^{-10}$	3.556	3.719	4.567	3.196		

Theoretical values at CISD level of theory are taken from [128]

[a]Experimental effective rotational constants and quartic centrifugal distortion constants obtained from [129]

[b]Experimental electric dipole moment from [130]

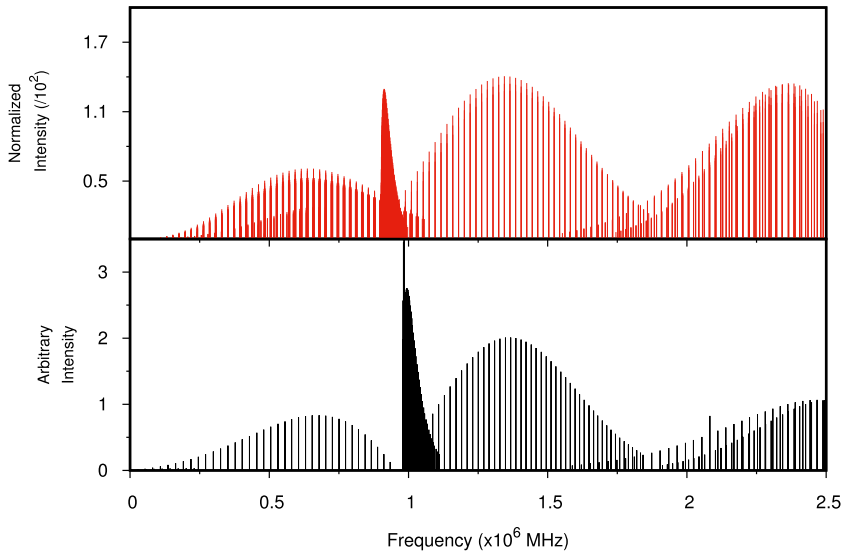

Fig. 5 Rotational spectrum of HNCO at 300 K simulated with mPW2PLYPD/aug-cc-pVTZ level of theory (black). The experimental spectrum is shown in red

centrifugal distortion effects felt by this molecule. The simulated spectra at B2PLYPD/aug-cc-pVTZ and B97D/aug-cc-pVTZ levels of theory are shown in the SI.

The simulated and experimental spectra follow the same profile throughout all values of J. However, due to the unusually large error associated with the predicted A_0 constant, calculated frequencies were significantly displaced in comparison with measured transitions. Overall, the mPW2PLYPD functional derived frequencies with discrepancies two orders of magnitude smaller than the ones obtained with B2PLYPD and B97D. More refined dispersion correction schemes and larger basis sets are likely to substantially improve those predictions.

Conclusions

In the present work, we briefly reviewed the most common model Hamiltonians to calculate the rotational spectroscopic constants of asymmetric tops beyond the rigid-rotor approximation. Those constants were used in the simulation of rotational spectra of some astrochemically relevant molecules. Spectroscopic constants calculated at DFT level of theory are overall close to measurements, resulting in rotational frequency predictions suitable for guiding laboratory experiments. Among the three chosen functionals, mPW2PLYP with dispersion corrections is the most successful in deriving effective rotational constants similar to measured values. In general, the GGA functional B97 with dispersion corrections predicted the most accurate quartic centrifugal distortion constants. However, its effective rotational constants are the furthest from experiment, resulting in the largest discrepancies in frequency predictions. Additionally, the B_0 and C_0 rotational constants have consistently been noted to play a dominant role in the simulations, being much more influential to the frequency predictions than the A_0 constant for both C_{2v} and C_s symmetry species.

Moreover, the theoretical description of the δ_K centrifugal distortion constant is likely to be neglecting important higher order terms, since its measured values are inconsistent with the other quadratic force field constants for H_2CO, H_2CS, c-HCOOH, and t-HCOOH. In the case of HNCO, the particularly strong centrifugal distortion is not described accurately enough at all levels of theory, requiring more refined theoretical treatments.

To the best of our knowledge, theoretical calculations of the centrifugal distortion constants of HNCO and c-HCOOH, as well as the effective rotational constants of c-HCOOH presented in this work, are being reported for the first time. The simulated spectra for the molecules considered here show a general good agreement with the experimental values, especially for transitions with J values up to 10, although the intensities are not so well reproduced in some cases.

Acknowledgements The authors acknowledge the National Laboratory for Scientific Computing (LNCC/MCTI, Brazil) for providing HPC resources of the SDumont supercomputer, which have contributed to the research results reported within this paper, and Fabio Cafardo for the help with coding and the dissertation of this text.

Funding The authors received financial support from Coordenação de Aperfeiçoamento de Pessoal de Nível Superior (CAPES) for financial support. Conselho Nacional de Desenvolvimento Científico e Tecnológico (CNPq).

References

1. Domenicano A, Hargittai I (1992) Accurate Molecular Structures: Their Determination and Importance. Oxford University Press, Oxford

2. Grubbs GS, Cooke SA (2010) J Mol Spectrosc 259(2):120–122
3. Costain CC (1969) Can J Phys 47(21):2431
4. Winton RS, Gordy W (1970) Phys Lett A 32(4):219–220
5. Winnewisser G, Lewen F, Thorwirth S, Behnke M, Hahn J, Gauss J, Herbst E (2003) Chem Eur J 9(22):5501–5510
6. Apponi AJ, McCarthy MC, Gottlieb CA, Thaddeus P (1999) J Chem Phys 111(9):3911–3918
7. McCarthy MC, Thorwirth S, Gottlieb CA, Thaddeus P (2004) J Am Chem Soc 126(13):4096–4097
8. Suma K, Sumiyoshi Y, Endo Y (2005) Science 308(5730):1885–1886
9. Koerber M, Baum O, Giesen TF, Schlemmer S, Hahn J, Gauss J (2009) Inorg Chem 48(5):2269–2272
10. Arumainayagam CR, Garrod RT, Boyer MC, Hay AK, Bao ST, Campbell JS, Wang J, Nowak CM, Arumainayagam MR, Hodge PJ (2019) Chem Soc Rev 48(8):2293–2314
11. McGuire BA, Martin-Drumel MA, Thorwirth S, Brünken S, Lattanzi V, Neill JL, Spezzano S, Yu Z, Zaleski DP, Remijan AJ, Pate BH, McCarthy MC (2016) Phys Chem Chem Phys 18(32):22693–22705
12. Belloche A, Garrod RT, Müller HSP, Menten KM (2014) Science 345(6204):1584–1587
13. Coutens A, Jørgensen JK, van der Wiel MHD, Müller HSP, Lykke JM, Bjerkeli P, Bourke TL, Calcutt H, Drozdovskaya MN, Favre C, Fayolle EC, Garrod RT, Jacobsen SK, Ligterinkx NFW, Öberg KI, Persson MV, van Dishoeck EF, Wampfler SF (2016) Astron Astrophys 590:L6
14. Spezzano S, Gupta H, Brünken S, Gottlieb CA, Caselli P, Menten KM, Müller HSP, Bizzocchi L, Schilke P, McCarthy MC, Schlemmer S (2016) Astron Astrophys 586:A110
15. Melli A, Melosso M, Tasinato N, Bosi G, Spada L, Bloino J, Mendolicchio M, Dore L, Barone V, Puzzarini C (2018) Astrophys J 855(2):123
16. Rivilla VM, Martín-Pintado J, Jiménez-Serra I, Zeng S, Martín S, Armijos-Abendaño J, Requena-Torres MA, Aladro R, Riquelme D (2019) Mon Not Rx Astron Soc 483(1):L114–L119
17. Belloche A, Garrod RT, Müller HSP, Menten KM, Medvedev I, Thomas J, Kisiel Z (2019) Astron Astrophys 628:A10
18. Beuther H, Zhang Q, Greenhill LJ, Reid MJ, Wilner D, Keto E, Shinnaga H, Ho PTP, Moran JM, Liu SY, Chang CM (2005) Astrophys J 632(1):355–370
19. Wyrowski F, Schilke P, Walmsley CM, Menten KM (1999) Astrophys J 514(1):L43–L46
20. Guzmán AE, Guzmán VV, Garay G, Bronfman L, Hechenleitner F (2018) Astrophys J Suppl 236(2):45
21. Goldsmith PF, Langer WD (1999) Astrophys J 517(1):209–225
22. Blake GA, Sutton EC, Masson CR, Phillips TG (1987) Astrophys J 315:621
23. Cazzoli G, Puzzarini C, Gambi A, Gauss J (2006) J Chem Phys 125(5):1–9
24. Puzzarini C, Biczysko M, Barone V, Peña I, Cabezas C, Alonso JL (2013) Phys Chem Chem Phys 15(39):16965–16975
25. Crabtree KN, Martin-Drumel MA, Brown GG, Gaster SA, Hall TM, McCarthy MC (2016) J Chem Phys 144(12):124201
26. Martin-Drumel MA, McCarthy MC, Patterson D, McGuire BA, Crabtree KN (2016) J Chem Phys 144(12):124202
27. Puzzarini C, Biczysko M, Barone V, Largo L, Pea I, Cabezas C, Alonso JL (2014) J Phys Chem Lett 5(3):534–540
28. McCarthy MC, Gottlieb CA, Gupta H, Thaddeus P (2006) Astrophys J 652(2):L141–L144
29. Écija P, Cocinero EJ, Lesarri A, Fernández JA, Caminati W, Castaño F (2013) J Chem Phys 138(11):114304
30. Calabrese C, Vigorito A, Maris A, Mariotti S, Fathi P, Geppert WD, Melandri S (2015) J Phys Chem A 119(48):11674–11682
31. Puzzarini C, Stanton JF, Gauss J (2010) Int Rev Phys Chem 29(2):273–367
32. Puzzarini C, Cazzoli G, Gauss J (2012) J Chem Phys 137(15):154311
33. Cernicharo J, McCarthy MC, Gottlieb CA, Agúndez M, Prieto LV, Baraban JH, Changala PB, Guélin M, Kahane C, Martin-Drumel MA, Patel NA, Reilly NJ, Stanton JF, Quintana-Lacaci G, Thorwirth S, Young KH (2015) Astrophys J 806(1):L3
34. Cazzoli G, Lattanzi V, Kirsch J, Tercero B, Cernicharo J, Puzzarini C (2016) Astron Astrophys 591:A126
35. Pawłowski F, Jørgensen P, Olsen J, Hegelund F, Helgaker T, Gauss J, Bak KL, Stanton JF (2002) J Chem Phys 116(15):6482–6496
36. Puzzarini C, Cazzoli G, López JC, Alonso JL, Baldacci A, Baldan A, Stopkowicz S, Cheng L, Gauss J (2011) J Chem Phys 134(17):174312
37. McCarthy MC, Gauss J (2016) J Phys Chem Lett 7(10):1895–1900
38. Spada L, Tasinato N, Vazart F, Barone V, Caminati W, Puzzarini C (2017) Chem Eur J 23(20):4876–4883
39. Puzzarini C, Heckert M, Gauss J (2008) J Chem Phys 128(19):194108
40. Townes CH, Schawlow AL (1975) Microwave Spectroscopy. Dover Publications, New York
41. Levine IN (1975) Molecular Spectroscopy. John Wiley & Sons, New York
42. Gordy W, Cook RL (1984) Microwave molecular spectra. John Wiley & Sons, New York
43. Puzzarini C, Barone V (2020) Phys Chem Chem Phys 22:6507–6523
44. Watson JKG (1968) Mol Phys 15(5):479–490
45. Rao KN, Mathews CW (1972) Molecular Spectroscopy: Modern Research. Academic Press, New York
46. Wilson EB, Howard JB (1936) J Chem Phys 4(4):260–268
47. Kneizys FX, Freedman JN, Clough SA (1966) J Chem Phys 44(7):2552–2556
48. Watson JKG (1968) J Chem Phys 48(10):4517–4524
49. Watson JKG (1977) vol 6. Elsevier, Amsterdam
50. Kivelson D, Wilson EB (1953) J Chem Phys 21(7):1229–1236
51. Watson JKG (1967) J Chem Phys 46(5):1935–1949
52. Aliev MR, Watson JKG (1976) J Mol Spectrosc 61(1):29–52
53. Watson JKG (1968) J Chem Phys 48(1):181–185
54. Becker R (1954) Introduction to Theoretical Mechanics. McGraw-Hill, New York
55. Nielsen HH (1941) Phys Rev 60:794–810
56. Nielsen HH (1945) Phys Rev 68(7-8):181–191
57. Nielsen HH (1951) Rev Mod Phys 23:90–136
58. Clabo DA, Allen WD, Remington RB, Yamaguchi Y, Schaefer HF (1988) Chem Phys 123(2):187–239
59. Jahn HA (1938) Proc R Soc Lond A 168(935):469–495
60. Kivelson D, Wilson EB (1952) J Chem Phys 20(10):1575–1579
61. Watson JKG (1966) J Chem Phys 45(4):1360–1361
62. Amat G, Goldsmith M, Nielsen HH (1957) J Chem Phys 27(4):838–844
63. Amat G, Nielsen HH (1957) J Chem Phys 27(4):845–850
64. Amat G, Nielsen HH (1958) J Chem Phys 29(3):665–672
65. Goldsmith M, Amat G, Nielsen HH (1956) J Chem Phys 24(6):1178–1182
66. Snyder LE, Buhl D, Zuckerman B, Palmer P (1969) Phys Rev Lett 22(13):679–681
67. Wollrab JE (1967) Rotational Spectra and Molecular Structure. Academic Press, New York
68. Becke AD (1997) J Chem Phys 107(20):8554–8560
69. Grimme S (2006) J Comput Chem 27(15):1787–1799
70. Grimme S (2006) J Chem Phys 124(3):034108

71. Schwabe T, Grimme S (2006) Phys Chem Chem Phys 8:4398–4401
72. Dunning TH (1989) J Chem Phys 90(2):1007–1023
73. Schlegel HB (2007) Optimization of Equilibrium Geometries and Transition Structures. John Wiley & Sons, Ltd, New York
74. Frisch MJ, Trucks GW, Schlegel HB, Scuseria GE, Robb MA, Cheeseman JR, Scalmani G, Barone V, Mennucci B, Petersson GA, Nakatsuji H, Caricato M, Li X, Hratchian HP, Izmaylov AF, Bloino J, Zheng G, Sonnenberg JL, Hada M, Ehara M, Toyota K, Fukuda R, Hasegawa J, Ishida M, Nakajima T, Honda Y, Kitao O, Nakai H, Vreven T, Montgomery JA, Peralta JE, Ogliaro F, Bearpark M, Heyd JJ, Brothers E, Kudin KN, Staroverov VN, Kobayashi R, Normand J, Raghavachari K, Rendell A, Burant JC, Iyengar SS, Tomasi J, Cossi M, Rega N, Millam JM, Klene M, Knox JE, Cross JB, Bakken V, Adamo C, Jaramillo J, Gomperts R, Stratmann RE, Yazyev O, Austin AJ, Cammi R, Pomelli C, Ochterski JW, Martin RL, Morokuma K, Zakrzewski VG, Voth GA, Salvador P, Dannenberg JJ, Dapprich S, Daniels AD, Farkas O, Foresman JB, Ortiz JV, Cioslowski J, Fox DJ (2009) Gaussian09 Revision A.01. Gaussian Inc. Wallingford CT
75. Western CM (2017) J Quant Spectrosc Radiat Transf 186:221–242
76. Downes D, Wilson TL, Bieging J, Wink J (1980) Astron Astrophys 40:379–394
77. Young KE, Lee J-E, Evans NJ II, Goldsmith PF, Doty SD (2004) Astrophys J 614(1):252–266
78. Araya E, Hofner P, Goss WM, Linz H, Kurtz S, Olmi L (2007) Astrophys J Suppl Ser 170(1):152–174
79. Leurini S, Parise B, Schilke P, Pety J, Rolffs R (2010) Astron Astrophys 511:A82
80. Mangum JG, Wootten A (1993) Astrophys J Suppl Ser 89:123
81. Martin JML, Lee TJ, Taylor PR (1993) J Mol Spectrosc 160(1):105–116
82. Johnson DR, Lovas FJ, Kirchhoff WH (1972) J Phys Chem Ref Data 1(4):1011–1046
83. Kondo K, Oka T (1960) J Phys Soc Jpn 15(2):307–314
84. Oka T, Morino Y (1961) J Phys Soc Jpn 16(6):1235–1242
85. Penzias AA, Solomon PM, Wilson RW, Jefferts KB (1971) Astrophys J Lett 168:L53
86. Oppenheimer M, Dalgarno A (1974) Astrophys J 187:231–236
87. Tieftrunk A, Pineau des Forets G, Schilke P, Walmsley CM (1994) Astron Astrophys 289:579–596
88. Palumbo ME, Geballe TR, Tielens AGGM (1997) Astrophys J 479(2):839–844
89. Savage BD, Sembach KR (1996) Annu Rev Astron Astrophys 34(1):279–329
90. Martín-Hernández NL, Peeters E, Morisset C, Tielens AGGM, Cox P, Roelfsema PR, Baluteau JP, Schaerer D, Mathis JS, Damour F, Churchwell E, Kessler MF (2002) Astron Astrophys 381:606–627
91. Howk JC, Sembach KR, Savage BD (2006) Astrophys J 637(1):333–341
92. García-Rojas J, Esteban C, Peimbert M, Costado MT, Rodríguez M, Peimbert A, Ruiz MT (2006) Mon Not R Astron Soc 368(1):253–279
93. Joseph CL, Snow J, Seab CG, Crutcher RM (1986) Astrophys J 309:771
94. Woods PM, Occhiogrosso A, Viti S, Kaňuchová Z, Palumbo ME, Price SD (2015) Mon Not R Astron Soc 450(2):1256–1267
95. Sinclair MW, Fourikis N, Ribes JC, Robinson BJ, Brown RD, Godfrey PD (1973) Aust J Phys 26:85
96. Liszt HS (1978) Astrophys J 219:454–457
97. Sutton EC, Blake GA, Masson CR, Phillips TG (1985) Astrophys J Suppl Ser 58:341–378
98. Cummins SE, Linke RA, Thaddeus P (1986) Astrophys J Suppl Ser 60:819
99. Minh YC, Irvine WM, Brewer MK (1991) Astron Astrophys 244:181
100. Charnley SB (1997) Astrophys J 481(1):396–405
101. Martin JML, Francois JP, Gijbels R (1994) J Mol Spectrosc 168(2):363–373
102. Sarka K, Demaison J, Margulés L, Merke I, Heineking N, Bürger H, Ruland H (2000) J Mol Spectrosc 200(1):55–64
103. Motiyenko RA, Margulés L, Alekseev EA, Guillemin JC, Demaison J (2010) J Mol Spectrosc 264(2):94–99
104. Clouthier DJ, Huang G, Adam AG, Merer AJ (1994) J Chem Phys 101(9):7300–7310
105. Fabricant B, Krieger D, Muenter JS (1977) J Chem Phys 67(4):1576–1586
106. Zuckerman B, Ball JA, Gottlieb CA (1971) Astrophys J Lett 163:L41
107. Winnewisser G, Churchwell E (1975) Astrophys J Lett 200:L33–L36
108. Liu SY, Girart JM, Remijan A, Snyder LE (2002) Astrophys J 576(1):255–263
109. Lefloch B, Ceccarelli C, Codella C, Favre C, Podio L, Vastel C, Viti S, Bachiller R (2017) Mon Not R Astron Soc 469(1):L73–L77
110. Favre C, Fedele D, Semenov D, Parfenov S, Codella C, Ceccarelli C, Bergin EA, Chapillon E, Testi L, Hersant F, Lefloch B, Fontani F, Blake GA, Cleeves LI, Qi C, Schwarz KR, Taquet V (2018) Astrophys J 862(1):L2
111. Hoyle F, Wickramasinghe NC (1999) Astrophys Space Sci 268:129–132
112. Basiuk VA (2001) J Phys Chem A 105(17):4252–4258
113. Redondo P, Largo A, Barrientos C (2015) Astron Astrophys 579:A125
114. Hocking WH (1976) Z Naturforsch Teil A 31:1113–1121
115. Demaison J, Herman M, Liévin J (2007) J Chem Phys 126(16):164305–164305
116. Winnewisser M, Winnewisser BP, Stein M, Birk M, Wagner G, Winnewisser G, Yamada KMT, Belov SP, Baskakov OI (2002) J Mol Spectrosc 216(2):259–265
117. Snyder LE, Buhl D (1972) Astrophys J 177:619
118. Churchwell E, Wood D, Myers PC, Myers RV (1986) Astrophys J 305:405
119. Kuan YJ, Snyder LE (1996) Astrophys J 470:981
120. Bisschop SE, Jørgensen JK, Bourke TL, Bottinelli S, van Dishoeck EF (2008) Astron Astrophys 488(3):959–968
121. Turner BE, Terzieva R, Herbst E (1999) Astrophys J 518(2):699–732
122. Zinchenko I, Henkel C, Mao RQ (2000) Astron Astrophys 361:1079–1094
123. Martín S, Requena-Torres MA, Martín-Pintado J, Mauersberger R (2008) Astrophys J 678(1):245–254
124. Martín S, Martín-Pintado J, Mauersberger R (2009) Astrophys J 694(1):610–617
125. Rodríguez-Fernández NJ, Tafalla M, Gueth F, Bachiller R (2010) Astron Astrophys 516:A98
126. Meier DS, Turner JL (2005) Astrophys J 618(1):259–280
127. Minh YC, Irvine WM (2006) New Astron 11(8):594–599
128. Defrees DJ, Loew GH, McLean AD (1982) Astrophys J 254:405–411
129. Yamada K (1980) J Mol Spectrosc 79(2):323–344
130. Hocking WH, Gerry MCL, Winnewisser G (1975) Can J Phys 53(19):1869–1901